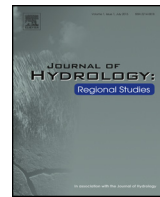




Contents lists available at ScienceDirect

## Journal of Hydrology: Regional Studies

journal homepage: [www.elsevier.com/locate/ejrh](http://www.elsevier.com/locate/ejrh)



# Spatiotemporal analysis of extreme precipitation events in the Northeast region of Argentina (NEA)

Miguel Lovino <sup>a,\*</sup>, Norberto O. García <sup>b</sup>, Walter Baethgen <sup>c</sup>

<sup>a</sup> Consejo Nacional de Investigaciones Científicas y Técnicas (CONICET), Facultad de Ingeniería y Ciencias Hídricas, Universidad Nacional del Litoral, CC 217, Ciudad Universitaria, 3000 Santa Fe, Argentina

<sup>b</sup> Facultad de Ingeniería y Ciencias Hídricas, Universidad Nacional del Litoral, CC 217, Ciudad Universitaria, 3000 Santa Fe, Argentina

<sup>c</sup> International Research Institute for Climate and Society, 61 Route 9W, Palisades, NY 10964, United States

## ARTICLE INFO

### Article history:

Received 9 April 2014

Received in revised form 28 August 2014

Accepted 5 September 2014

### Keywords:

Extreme precipitation events (EPE)  
Northeast region of Argentina (NEA)  
Standard Precipitation Index (SPI)  
Principal Component Analysis  
Hydrological dry/wet events  
Vulnerability

## ABSTRACT

**Study region:** An area in NEA located within the La Plata Basin (LPB) where extreme precipitation events (EPE) are the most harmful and costly natural disasters.

**Study focus:** The study analyzes the spatiotemporal behavior of EPE through a Principal Component Analysis (PCA) applied to fields of Standard Precipitation Index (SPI) at different time scales. The vulnerability of the NEA to EPE was estimated by defining the portion of the region experiencing extremely dry/wet conditions in critical months. Singular Spectrum Analysis (SSA) was applied to the time series looking for significant trends or oscillatory modes. **New hydrological insights for the region:** The spatial average SPI series show a positive nonlinear trend with changes to wetter conditions from 1960 to 2000s, subsequent signs of stabilization and a trend reversal since 2007. The most severe hydrological and agricultural droughts occurred between 1901 and 1960 while the larger wet EPE were recorded between 1970 and 2005. Moreover, a prolonged dry period was registered between 1921 and 1939 that might extend the "Pampas Dust Bowl" to the bulk of the NEA. The EPE show cycles of 6.5 and 8.7 years together with a quasi-decadal cycle in the Northwestern corner. Our results suggest that almost the entire NEA is highly vulnerable to EPE at a time scale relevant for agricultural activities and the Central-West portion is particularly vulnerable to hydrological EPE.

© 2014 The Authors. Published by Elsevier B.V. This is an open access article under the CC BY-NC-ND license (<http://creativecommons.org/licenses/by-nc-nd/3.0/>).

\* Corresponding author at: Ruta Nacional N° 168 – Km 472.4, CC 217, Ciudad Universitaria, 3000 Santa Fe, Argentina.  
Tel.: +54 342 457 5233x176.

E-mail addresses: [mlovino@unl.edu.ar](mailto:mlovino@unl.edu.ar) (M. Lovino), [ngarcia@unl.edu.ar](mailto:ngarcia@unl.edu.ar) (N.O. García), [baethgen@iri.columbia.edu](mailto:baethgen@iri.columbia.edu) (W. Baethgen).

## 1. Introduction

Persistent EPE such as drought and wetness are the most damaging and costly natural disasters (Wilhite, 2000). Droughts and floods have different impacts in soil moisture, groundwater supplies, streamflow and reservoir levels; affecting a wide range of sectors such as agriculture, commerce, hydropower, and many others. According to Magrin et al. (2007), the Argentinean Pampas have experienced important increases in rainfall that have had impacts on land use and crop yields and have increased flood frequency and intensity during the last decades of the 20th century. Furthermore, increased precipitation has led to increased river discharge (García and Vargas, 1998), since evaporation seems to not have changed too much (Berbery and Barros, 2002). In addition, increase in the vulnerability to larger wet events, with more than 30% of the La Plata Basin (LPB) under water excess, has been observed after 1950 (Krepper and Zucarelli, 2010). On the other hand the frequencies of extreme droughts have also increased during the last 25 years: Cavalcanti et al. (2011) suggested that some regions of LPB have presented a trend of increased dryer conditions from the mid-1980s, in agreement with the occurrence of severe droughts during the years 1988/89, 1995/96 and 2008/09.

Regarding climate forcing, Seager et al. (2010) have showed that both, tropical Pacific and Atlantic global sea surface temperatures (SSTs) contribute to southeast South America (SESA) precipitation variability, with the former dominating in the interannual time scale and the latter dominating in longer time scales. They argued that cold tropical Atlantic SST anomalies seem to cause wet conditions in SESA and that the wetting trend of the last years of the 20th century was largely forced by a relative cooling of the tropical Atlantic Ocean related to the cool phase of the Atlantic Multidecadal Oscillation (AMO). In addition, the models participating in the Intergovernmental Panel on Climate Change Fourth Assessment Report (IPCC AR4, Meehl et al., 2007) predict a weak increase in SESA precipitation over the 20th century as a consequence of anthropogenic climate forcing that could explain some of the observed wet trend in SESA. However, Vera et al. (2010) showed that evidence of observed decadal variability makes clear that the anthropogenic climate change signal at the regional level may be strongly modulated by natural climate variations. On the other hand, several studies have linked SESA precipitation in interannual time scales to the El Niño–Southern Oscillation (ENSO), with El Niño conditions showing increased precipitation (e.g., Paegle and Mo, 2002) and leading to increased streamflow in the rivers (e.g., Robertson and Mechoso, 1998).

In this paper we consider an area in NEA characterized by homogeneity in relief, climate and natural resources, delimited by  $-26.25^\circ < \text{lat} < -35.75^\circ$ ,  $-58.25^\circ < \text{lon} < -64.75^\circ$  (Fig. 1b). The study area is located within the Argentine Litoral and West and South borders of the LPB—according to the divisions proposed by Caffera and Berbery (2006)—and covers a large portion of the Low Paraná sub-basin and important territories of the Salado River Basin (Fig. 1a and b). The water resources in these basins include a highly productive region where the main economic activities are cereal production and livestock. The Low Paraná River presents very low coasts and therefore, the very high discharges cause severe floods (Coronel and Menéndez, 2006). The largest flood of the Paraná River in the 20th century occurred in 1983, when more than 100,000 people had to be evacuated and economic losses amounted to more than one billion dollars (Krepper and Zucarelli, 2010). Additionally, the Salado river—a tributary of the Paraná river—experienced the most catastrophic flood in April 2003, causing economic losses of approximately US\$ 1000 million (ECLAC, 2003) and affecting nearly one-third of the population of Santa Fe city (140,000 inhabitants).

An analysis of precipitation characteristics is a critical component for the management of climate risk (Bordi et al., 2009). In the recent years, the SPI (McKee et al., 1993) has been widely used and highlighted for a number of advantages over other indices (Guttman, 1999; Keyantash and Dracup, 2002). Thus, SPI has been accepted by the World Meteorological Organization (WMO) as the reference index for more effective drought monitoring and climate risk management (Hayes et al., 2011). Furthermore, SPI was designed to quantify the precipitation deficit/excess for multiple time scales, which reflect the impact of drought and wetness on the availability of different water resources. Shorter time scales (weeks to months) are used to characterize meteorological conditions, important to agricultural activities since soil moisture has a relative fast response to precipitation anomalies. Longer-term time scales (from seasons to years) are used to monitor hydrological settings, significant

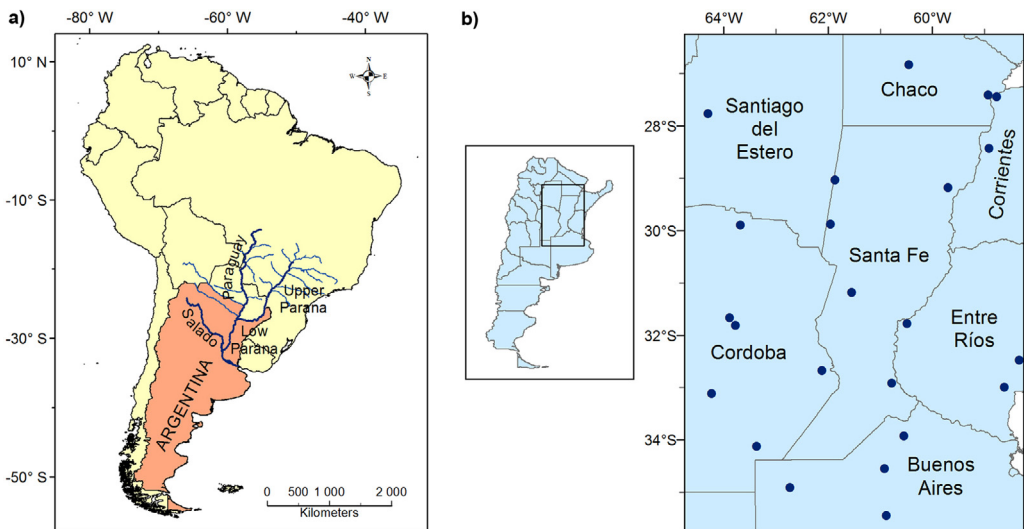


**Fig. 1.** (a) South America and the main rivers of SESA. (b) The study area with Argentine provinces and stations with monthly observed precipitation chosen considering their record length and completeness.

in water supply management since groundwater, streamflow, and reservoir storage reflect the longer-term precipitation anomalies (Sirdaş and Şen, 2003).

Several studies have analyzed the spatiotemporal evolution of SPI at different time scales for diverse regions (Lloyd-Huges and Saunders, 2002; Sönmez et al., 2005; Vicente-Serrano, 2006; Livada and Assimakopoulos, 2007; Zhai et al., 2010). Another set of papers have identified trends and periodicities of dry and wet periods in the temporal series of drought/wet indices in many regions of the world (Bordi et al., 2004, 2009; Santos et al., 2010; Raziei et al., 2010; Bordi and Sutera, 2012; Fischer et al., 2013; Telesca et al., 2013). In the SESA region, Krepper and Sequeira (1998) found evidence of a sustained positive precipitation trend from the 1950 onwards in Northeast and Central Argentina, almost all of Uruguay and a very small region of the state of Rio Grande do Sul in Brazil. Furthermore, Krepper and Garcia (2004) present evidence that precipitation in the LPB show cycles in the interannual frequency band with about 6 and 3.5 years and a quasi-biennial oscillation. In addition, Venencio and García (2005) suggested that the frequency of droughts seems to have been decreasing throughout the whole humid Argentinean Pampa region since 1970, with an average of one drought every 3 years until 1969, and one drought every 5 years from then onward.

In assessing drought (wetness) risk, the first step is EPE monitoring and the understanding of the spatial extent and temporal variability of dry (wet) events, also in relation to a changing climate. Future anticipated increases in climate variability and changes in the frequency and magnitude of extreme weather events may perturb the existing hydrologic system, with greatest impacts falling upon sectors most vulnerable to these changes. Considering the possible future increase in extreme events, it is essential to establish new methods to manage the natural systems for achieving sustainability and change the current strategy of crisis management to risk management. An analysis that can help to identify the type of information needed to assist decision-making and to improve adaptation and risk management policies and practices is an estimation of regional climate EPE at different temporal scales observed throughout the last century and up to the present. This analysis and an adequate strategy for water resources management could minimize the severity of the impacts due to drought and floods in the region.

The general objective of our paper is to analyze the spatiotemporal EPE, characterizing dry and wet conditions by means of SPI on multiple time scales, between 1901 and 2010 in the NEA. The investigation is focused on hydrological dry/wet events and its impact on the region. In addition, the vulnerability of the NEA to EPE is estimated by defining the portion of the region experiencing water

excess/deficit conditions at different time scales and determining the zones that were historically most affected by extreme events and their mean magnitude and severity. This information will contribute to enhance water management and improve the design of adaptive measures.

In the following section, we introduce the precipitation data and the methodology that includes SPI estimation, PCA and SSA. In Section 3, we present the results for the spatiotemporal behavior of dry and wet EPE and the spatial extent of extreme drought and wetness. Finally, some implications of the findings are discussed in Section 4 and the concluding remarks are presented in Section 5.

## 2. Data and methods

### 2.1. Precipitation data

We used monthly observed precipitation data from 23 meteorological stations from the National Weather Service and National Institute of Agricultural Technology in Argentina. The stations were chosen considering their record length and completeness, the absence of gaps and the data quality. Stations in the NEA are not homogeneously distributed in space (see Fig. 1b), and therefore we used the following high-resolution ( $0.5^\circ \times 0.5^\circ$ ) gridded precipitation datasets: the Climatic Research Unit time-series dataset version 3.2 (CRU TS 3.2, Jones and Harris, 2012), spanning 1901–2011 and the Global Precipitation Climatology Centre dataset version 6 (GPCC v6, Schneider et al., 2011) from 1901 to 2010.

The process of selection of the precipitation series used in this paper is based on the stability of the meteorological stations and in the confidence in the measurements as evidenced by tests of coherence and consistency: Kolmogorov–Smirnov (Von Storch and Zwiers, 1999) and double mass curves of doubly accumulated precipitation (Remenieras, 1974). Furthermore, the degree of randomness in the time series was assessed by the accumulated periodogram method (Anderson, 1977). Moreover, the selection process of the time series satisfies the requirements of quality control stated in Chapter 9 of the WMO Guide to Hydrological Practices (WMO, 2008). The gridded datasets were validated with observed precipitation by creating average spatial time series (Fig. 2). The mean values of the series are 941 mm in the observed series, 925 mm in GPCC v6 dataset and 868 mm in CRU TS 3.2. We also calculated the Pearson correlation coefficients between average spatial time series of observed data and the gridded datasets. For the total period of our paper (1901–2010), the correlation coefficient between observed data and GPCC v6 ( $r=0.946$ ) was quite similar to the correlation with CRU TS 3.2 ( $r=0.943$ ). Both Pearson correlation coefficients are statistically significant at the 0.01 confidence level. The 99% confidence interval for  $r$  is computed from the probability points of the standard normal distribution (Chatfield, 2004). Fig. 2 shows that differences between observed values and GPCC v6 data (approximately 24 mm in the mean value) are smaller than the differences with CRU TS 3.2 (72 mm) in spatial average each year, with the largest differences in the early years of the twentieth century.

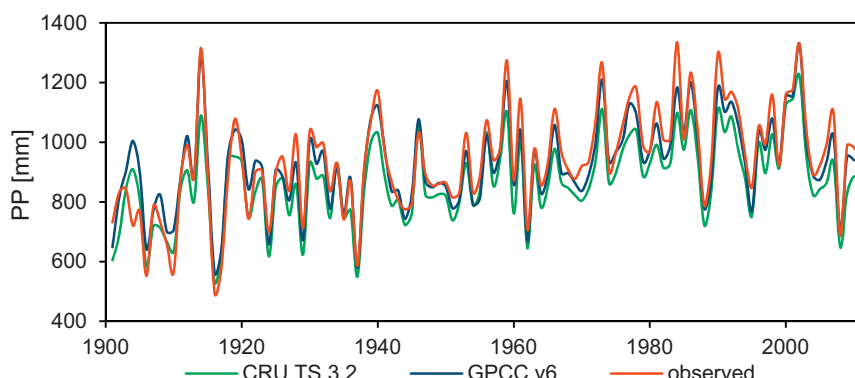


**Fig. 2.** Time series of spatial average annual precipitation in the entire box.

**Table 1**

Classification scales by SPI value according to Agnew (2000) and corresponding event probabilities.

SPI value	Probability (%)	Category
>1.65	5	Extremely wet
1.28 to 1.64	5	Very wet
0.84 to 1.28	10	Moderately wet
-0.84 to 0.84	60	Near normal
-0.84 to -1.28	10	Moderately dry
-1.28 to -1.64	5	Very dry
<-1.65	5	Extremely dry

The average spatial time series of the CRU TS 3.2 underestimates the mean precipitation values over the entire period, while GPCC v6 data fit best the extreme fluctuations.

Comparisons of time series of gridded data (CRU TS 3.2 and GPCC v6) with observed data in grid points near the precipitation weather stations were also performed (not shown). These comparisons indicated that the GPCC v6 data were better correlated with observations and presented smaller mean errors in different sectors of the study area. In addition the GPCC v6 dataset satisfy the reliability criteria of climate data to investigate dry/wet periods: (i) ease to access, (ii) uniform coverage of the area of interest, (iii) temporal duration long enough to be statistically trustworthy, and (iv) it has the ability to capture dry and wet events (Bordi et al., 2006). Based on these considerations and the results of validations we present only the results obtained with the GPCC v6 database.

## 2.2. Standard Precipitation Index

The SPI is constructed with the precipitation field and its computation for any location is based on the long-term precipitation record accumulated over the selected time scale. The long-term record is fitted to a probability distribution (usually a Gamma distribution), which is then transformed through an equal-probability transformation into a normal distribution (Raziei et al., 2010). A particular precipitation total for a specified time period is then identified with a specific SPI value consistent with its probability. Positive SPI values indicate greater than median precipitation, while negative values indicate less than median precipitation. The magnitude of departure from zero indicates the probability of occurrence and therefore, plans and decisions can be made based on this SPI value (Hayes et al., 1999). A detailed description of SPI calculation can be found in Edwards and McKee (1997), Lloyd-Huges and Saunders (2002) or Bordi and Sutera (2012), among others.

The intensity of wet and dry EPE can be defined according to the classification system proposed by Agnew (2000) (Table 1), using probabilities of occurrence to define classes. Thus, at a given location, a very wet (dry) month will have a probability of occurrence of 10% and an extremely wet (dry) month 5%. Hence very wet (dry) conditions are only expected 1 year in 10 and extremely wet (dry) conditions in 1 year out of 20.

Monthly precipitation series from GPCC v6 were transformed for each grid point into SPI<sub>n</sub> (t) series for n=6, 12, and 18 months. In this paper, meteorological dry/wet condition have been assessed through SPI<sub>6</sub> (t) as an indicator of short-term EPE for agricultural application, while SPI<sub>12</sub> (t) and SPI<sub>18</sub> (t) series, are used to investigate hydrological conditions. The main interest of this paper is to detect patterns of long-term EPE and their hydrological impacts and therefore, it focuses on hydrological dry/wet events analyzed with SPI for 18-months. Bordi et al. (2004, 2009) argued that a time scale of 18 month capture the low frequency variability and filters out the effects on drought and wetness of short-term periodicities and seasonal cycles.

## 2.3. Principal Component Analysis and Singular Spectrum Analysis

We used the PCA (Von Storch and Zwiers, 1999; Wilks, 2006) to the SPI<sub>n</sub> (t) series to analyze the patterns of droughts/wetness co-variability. The SPI at single grid points as variables ( $X_i$ ) and the time periods as individuals has been used in what is commonly known as S-mode. This method allows to obtain the Principal Component (PCs) as signals or time series and the eigenvectors ( $u_{ij}$ ) as spatial

patterns, which vary in time according to the PCs. The variable correlation matrix was used in the PCA because we want to determine the spatial relationships between variables (SPI series at each grid point) more than the internal variability in each SPI series. Then, we assessed the spatial distribution of the correlation for each variable (SPI time series at a single grid point) with each of the first PCs. These representations are equivalent to the traditional eigenvectors patterns and have a more direct interpretation for the reader. The use of a correlation matrix, defined by:

$$A = [a_{ij}] \quad \text{where } a_{ij} = \text{Corr}(X_i, PC_j) \quad (1)$$

allows the rapid calculation of the proportion of variance of variable  $X_i$  accounted for by the  $k$  first PCs through the addition  $a_{i1}^2 + a_{i2}^2 + \dots + a_{ik}^2$  (Krepper and Sequeira, 1998).

The temporal behavior of PCs was analyzed with SSA (Ghil et al., 2001; Wilks, 2006) in the low frequency band (LFB), with the objective of determining the structures of trend and oscillatory modes in  $SPI_n(t)$  series. SSA is applied in the time domain and aims to describe the variability of a discrete and finite time series  $X_i^* = X^*(i\Delta t)$ , ( $i = 1, \dots, N$  and  $\Delta t$  = sampling interval) in terms of its lagged autocovariance structure. Variables are normalized to  $X_i = X(i\Delta t)$  and lagged autocovariance matrix  $C$  ( $M \times M$ ) is defined:

$$C_{ij} = \frac{1}{N-M} \sum_{s=i}^{N-M+|i-j|} X_s X_{s+|i-j|} \quad (i, j = 1, \dots, M) \quad (2)$$

where  $M$  is the temporal embedding dimension (windows length) over which the covariance is defined and  $\tau = M\Delta t$  maximum delay (lag).

The eigenvalue decomposition of the lagged autocovariance matrix  $C$  ( $M \times M$ ), up to lag  $M\Delta t$ , produces temporal-empirical orthogonal functions  $T\text{-EOF} = [T\text{-EOF}_1, \dots, T\text{-EOF}_M]$  with  $T\text{-EOF}_k = [E_k(1), \dots, E_k(M)]^T$  and temporal-principal components  $T\text{-PC} = [T\text{-PC}_1, \dots, T\text{-PC}_{N-M}]$  with column vectors defined as  $T\text{-PC}_k = [PC_k(1), \dots, PC_k(N-M)]^T$  statistically independent, with no presumption as to their functional form. Each  $T\text{-PC}$ s has a variance  $\lambda_s$  (eigenvalue) and represents a filtered version of the original series  $X_i$ . A key issue in SSA is the proper choice of  $M$ . Von Storch and Navarra (1995) recommended not to exceed  $M = N/3$  and explain that SSA is typically successful at analyzing periods in the range  $(M/5, M)$ . In this paper, a window length of  $M = 360$  months (30 years) was used because it provides a statistically significant estimate of the periods of low frequency that can be found in the series of  $SPI_n(t)$ .

The entire time series or the part of it that corresponds to trends or oscillatory modes can be reconstructed by using linear combinations of principal components and eigenvectors, as:

$$X_i = X(i\Delta t) = \frac{1}{M} \sum_{k=1}^M \sum_{i+j=s} [(PC)_k(i)][(E)_k(j)] \quad (3)$$

where  $k$  is the set of T-EOFs on which reconstruction is based.

The basic idea in SSA is simple: a PCA is done with the variables analyzed being lagged versions of a single time series variable. We construct an input matrix that contains the “lagged” time series  $X^*(i\Delta t)$  where  $i = 1, \dots, N$  are the lags and  $\Delta$  is the time increment (the “size” of the lag). The lagged covariance matrix  $C_{ij}$  (Eq. (2)) contains covariances between the time series at all possible combinations of lags. The T-PCs obtained by the decomposition of  $C_{ij}$  can be interpreted as moving averages of the original time series, the averages being weighted by the coordinates of the T-EOFs. The decomposition in PCs given in Eq. (3) allows us to identify the different hidden processes in the signal  $X^*(i\Delta t)$ . The first T-PCs will be naturally associated with deterministic mechanisms that account for most of the variance of the series. The remaining T-PCs correspond to information that cannot be separated from the background noise.

In this paper, the spatiotemporal behavior of periods of excess and water deficit was determined through a PCA applied to the fields of SPI at different time scales. The vulnerability of the region to EPE was determined by defining the spatial extent of these periods by means of the percentage of grid points in wet or dry conditions for each month of the time series. SSA was applied to the time series of interest looking for significant signals in the LFB (trends or oscillatory modes).

### 3. Results

#### 3.1. Spatiotemporal behavior of dry and wet extreme precipitation events

PCA was applied to the field of  $SPI_n(t)$  ( $n = 6, 12$  and  $18$  month) to define the spatial distribution of  $a_{ij}$  correlations for SPI time series at each grid point with the principal components  $PC_j$  ( $j = 1, 2, 3$ ). The temporal behavior of the  $PC_j(t)$ ,  $j = 1, 2, 3$ ;  $n = 6, 12$  and  $18$  months series was determined by applying SSA, looking for low frequency signals in the LFB and using a window length  $M$  of  $360$  months ( $30$  years).

The first PC explained a high percentage of the total variance for all  $SPI_n(t)$  time series analyzed (49.5%, 52.7% and 54.7% for  $n = 6, 12$  and  $18$  month, respectively). Correlation of  $PC_1(t)$  with SPI time series at each grid point, expressed by  $a_{i1}$ , resulted in positive values in all cases, proving to be the component that is closest related with variables (SPI time series). We determined the correlation of the  $PC_1$  with each SPI spatial average time series in the region ( $SPI_n(t)$ ,  $n = 6, 12$  and  $18$  months). The obtained coefficients in all cases were close to 0.999, indicating that the average areal behavior of SPI fields could be explained by  $PC_1(t)$  series. At all time scales analyzed, the T-PC1 is associated with a nonlinear trend that explains different proportions of total variance for each  $PC_1(t)$ .

**Fig. 3a** and b shows the  $PC_{16}(t)$  and  $PC_{12}(t)$  of the  $SPI_6(t)$  and  $SPI_{12}(t)$  time series, together with the partial reconstruction corresponding to the nonlinear trends  $TEN_6(t)$  and  $TEN_{12}(t)$ , based in T-EOF1 and T-PC1 for both series, accounting for 8% and 16% of the variances, respectively. The low-frequency behavior of trend series shows a shift to wetter conditions for the period 1960–2000s. **Fig. 3a** and b shows a period with a great number of wet EPE between 1970 and 2000. The precipitation wet extremes show signs of stabilization starting in the first decade of 21st century, beginning to decline significantly since 2007. This behavior suggests that wet EPE of high intensity and duration noted between 1970 and 2003 (represented by SPI series at scales of 6 and 12 months) began to decline in the last years of the 2000s. In addition,  $PC_{16}(t)$  and  $PC_{12}(t)$  series indicate that the droughts, particularly relevant for the agricultural sector (long duration and severity), were more frequently observed in the early 20th century, although there was an extreme drought in the years 2008–2009 that caused serious damage to the economic activities of the region. It should be stressed that the spatial patterns of the  $PC_{16}$  and  $PC_{12}$  are similar to those presented in **Fig. 4a–c**, corresponding to the  $PC_{18}$ .

Even though spatial patterns obtained from PCA were very similar for the three time scales analyzed, we present in this paper the complete analysis for  $SPI_{18}(t)$ , selected because of the representativeness results and to focus in the low frequency behavior of extreme wet and dry periods and their hydrological impacts. **Fig. 4a** shows the correlation of the  $PC_{18}(t)$ , which accounts for 54.7% of the total variance, with  $SPI_{18}(t)$  series at each grid point used as variables, that is  $a_{18i1}$ . Positive correlation values are observed throughout the region, with correlations higher than 0.65, except in the Northwest corner, providing evidence that most of the study area has  $SPI_{18}(t)$  series whose low-frequency

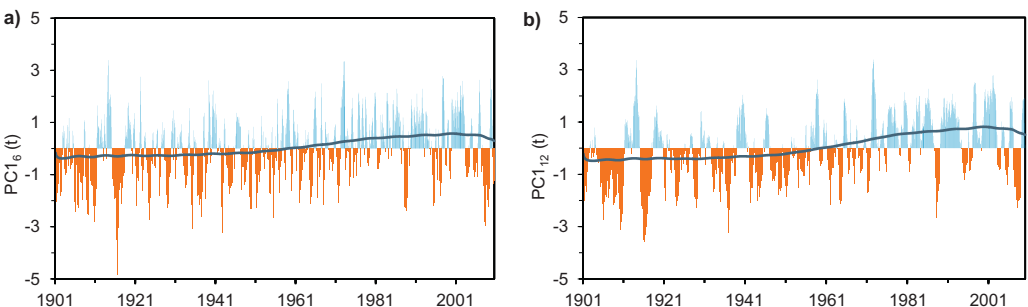


**Fig. 3.**  $PC_1(t)$  from PCA of  $SPI_n(t)$  fields that explain its areal average temporal behavior. Solid lines denote the partial reconstruction corresponding to the nonlinear trends  $TEN_n(t)$  derived from SSA. (a)  $PC_{16}(t)$  and  $TEN_6(t)$  (accounting for 8% of the total variance). (b)  $PC_{12}(t)$  and  $TEN_{12}(t)$  (accounting for 16% of variance).

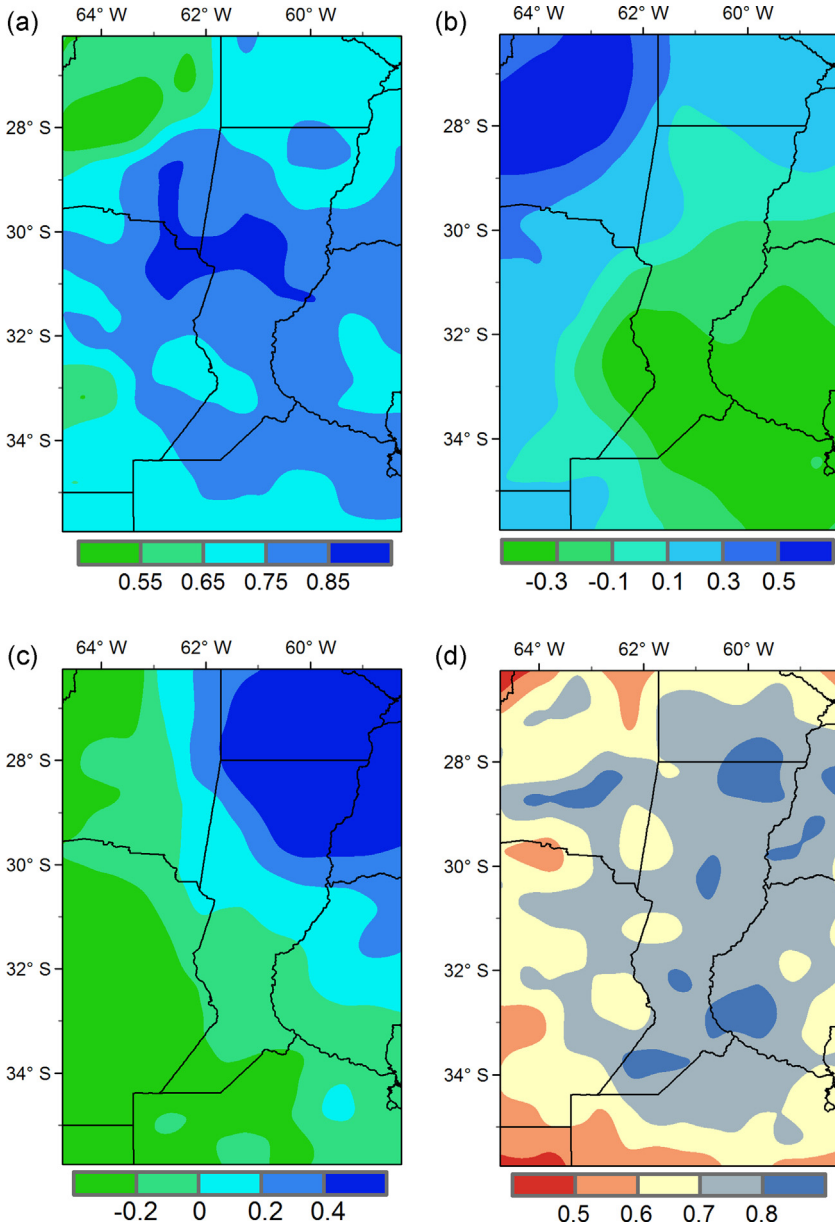


**Fig. 4.** Spatial distribution of (a)  $a18_{i1}$ , (b)  $a18_{i2}$  and (c)  $a18_{i3}$ . (d) Portion of the total variance of the  $SPI_{18}(t)$  at each grid point represented by  $PC_{j18}(t)$ ,  $j = 1, 2$  and  $3$ .

time responses are well represented by a signal like the  $PC_{18}(t)$  (Fig. 5a). The maximum values of  $a18_{i1}$  (over 0.85) are situated in the North-Centre of the Santa Fe, Northeast of Córdoba and Southeast of Santiago del Estero provinces in Argentina, where more than 72% of the  $SPI_{18}$  time series variance is explained by the  $PC_{18}(t)$ .

Table 2 summarizes the modes detected by SSA in  $PC_{j18}(t)$  series using a windows length  $M = 360$  months. Specifically in the analysis of  $PC_{18}(t)$  series, T- $PC_1$  is associated with a nonlinear trend

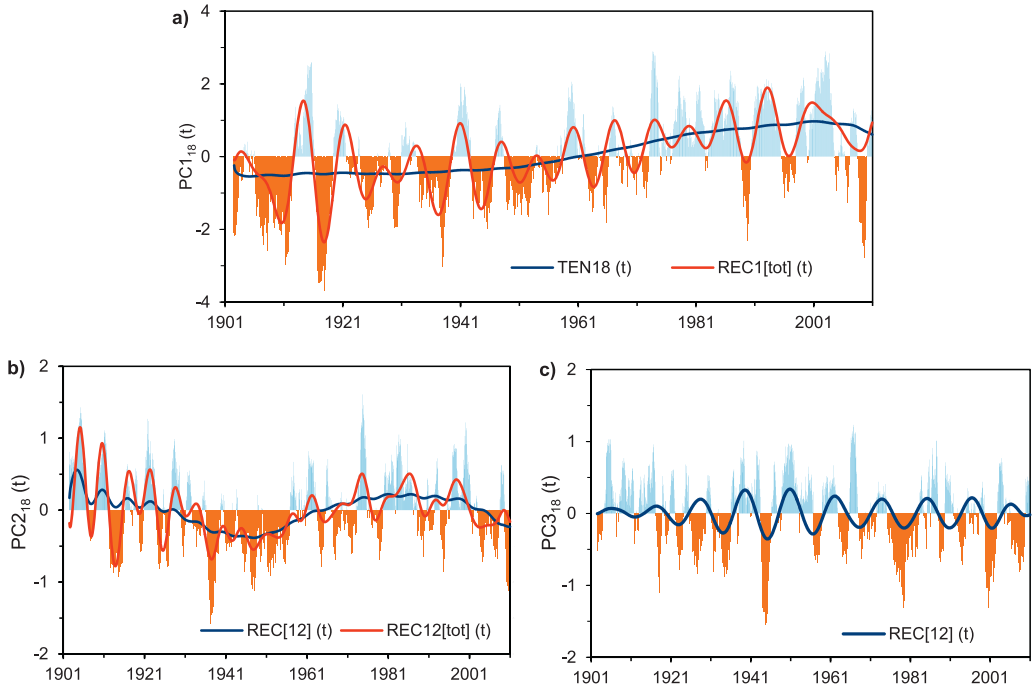


**Fig. 5.** (a)  $\text{PC1}_{18}(t)$  from PCA of  $\text{SPI}_{18}(t)$  fields that explain its areal average temporal behavior. Solid lines denote the partial reconstruction corresponding to the nonlinear trend [ $\text{TEN18}(t)$ ] and the partial reconstruction of filtered series,  $\text{REC1[tot]}(t)$ . (b)  $\text{PC2}_{18}(t)$  from PCA of  $\text{SPI}_{18}(t)$ .  $\text{REC12}(t)$  corresponds to the very low frequency mode based on T-PC1 and T-PC2 and  $\text{REC12[tot]}(t)$  represent the partial reconstruction of filtered series. (c)  $\text{PC3}_{18}(t)$  from PCA of  $\text{SPI}_{18}(t)$  series. Solid line denote the partial reconstruction  $\text{REC12}(t)$  of the cycle with  $T=11.2$  years.

which explains 22% of the total variance of the series. Furthermore, we detect oscillatory pairs with dominant periods  $T=6.5$  years and  $T=8.7$  years. The periods were obtained by computing the power spectrum of the PCs for each oscillatory mode. To calculate the power spectrum we first compute the autocovariance of the time series and then we perform the Fourier transform to obtain an unsmoothed power spectrum estimate. After that, this estimate is smoothed using a Hamming window. The lag  $L$

**Table 2**

Trends and significant low-frequency oscillatory pairs obtained from applying SSA ( $M=360$  months) to the principal components of  $\text{SPI}_{18}$  field, with the percentage of explained variance and correlation coefficient  $R$ .

Principal component $\text{PCj}_{18}(t)$	Oscillatory pair (components)	Trend or dominant period (year/cycle)	Explained variance (%)	$R$ at lag $L$ (month)
$\text{PC1}_{18}(t)$	T-PC1	Trend	22	
	T-PC2 and T-PC3	6.5	20.7	-0.987; $L=20$
	T-PC4 and T-PC5	8.7	13	0.922; $L=26$
	T-PCs [1 + 2 + 3 + 4 + 5]		55.7	
$\text{PC2}_{18}(t)$	T-PC1 and T-PC2	Approx. 80 (out of range)	21.5	
	T-PC3 and T-PC4	6	13.8	0.761; $L=18$
	T-PC5 and T-PC6	11.25	11	-0.821; $L=34$
	T-PCs [1 + 2 + 3 + 4 + 5 + 6]		46.3	
$\text{PC3}_{18}(t)$	T-PC1 and T-PC2	11.2	14.9	-0.951; $L=33$

value with the highest correlation coefficient  $R$  was found at approximately  $T/4$  (see Table 2). Thus, it is assumed that both eigenvectors as the T-PCs that define the oscillatory pairs are in quadrature. Fig. 5a presents the partial reconstruction of the nonlinear trend  $\text{TEN}_{18}$  (t), based on T-PC1 and T-EOF1, and filtered series  $\text{REC1[tot]}$  (t), corresponding to the partial reconstruction with the trend and the two oscillatory modes that were detected with SSA. The  $\text{TEN}_{18}$  (t) series features a clear long-term change to positive values from the 1960s, presenting a humid period until 2000 where a negative change is observed, increasing from the year 2008.

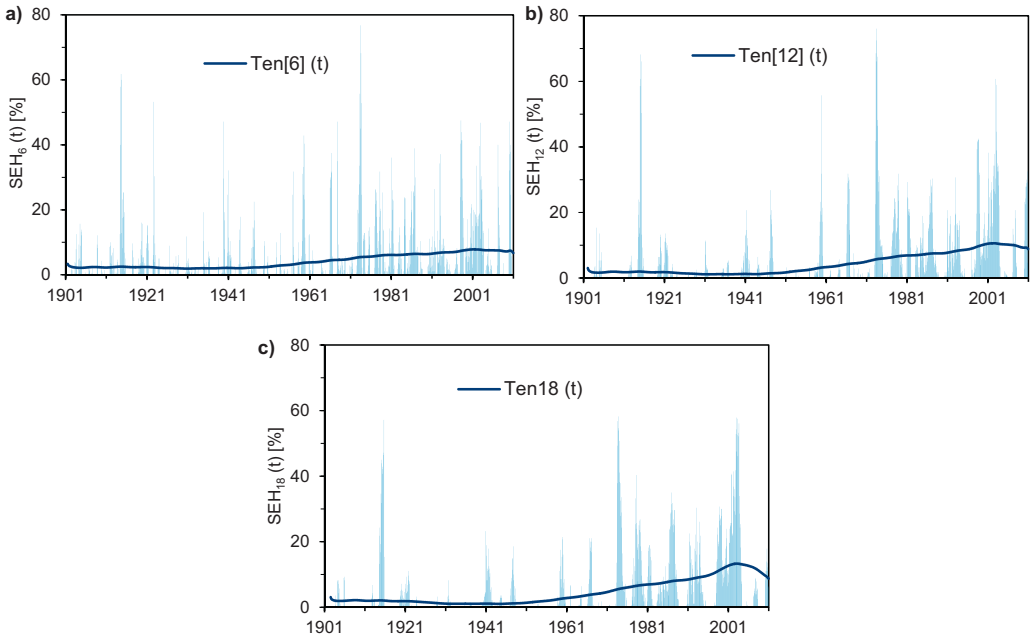
The  $\text{PC1}_{18}$  (t) series (Fig. 5a) indicates that the largest and most frequent hydrological droughts in the NEA occurred between 1901 and 1960, with a clearly differentiated period of long duration and high intensity wet EPE between years 1970 and 2005. We note an extended period of negative  $\text{SPI}_{18}$  (t) values between 1924 and 1939 interrupted only by positive values in the normal range between the months of December 1930 to June 1932. The most intense drought events were recorded in the early twentieth century: between January 1906 and June 1912 (mean intensity of  $\text{SPI}_{18}$  (t) = -1.65) with 78 consecutive months of duration, and between March 1916 and April 1919 (mean intensity of  $\text{SPI}_{18}$  (t) = -2.17) with 38 months of duration. Both events are congruent with La Niña periods according to a historical analysis of Southern Oscillation Index (SOI, Trenberth and Hoar, 1996) time series. On the other hand, the most intense wet events were recorded in the last 30 years of the 20th century, with extraordinary peaks in April 1973 and November 2002. The former is consistent with strong El Niño event while the latter coincides with a moderate El Niño event, defined according to the Oceanic Niño Index (ONI, 3-month mean SST anomaly for the Niño 3.4 region, NOAA/NWS/CPC). It should be emphasized that we used SOI time series for determining the intensity of El Niño/La Niña events before 1950 and, from then on, we use ONI. These two indices are common methods used for determining the intensity of ENSO and have similar shapes but of opposite sign. The SOI is based on the difference between sea level pressures at Tahiti and Darwin, Australia and the ONI is based on sea surface temperatures in the eastern equatorial Pacific Ocean, whose data record starts at 1950.

Fig. 4b presents the pattern of correlation of the  $\text{SPI}_{18}$  (t) series in each grid point with  $\text{PC2}_{18}$  (t). A maximum value of positive correlation with relative importance ( $a_{18,2} \max = 0.56$ ) is situated in the Northwestern corner of the region. The  $\text{PC2}_{18}$  (t) series accounts for the 9.5% of the total variance and Fig. 5b shows its evolution with time. The results of applying SSA to  $\text{PC2}_{18}$  (t) series are shown in Table 2, where we can see an oscillatory mode of very low frequency (out of the range allowed by the windows length) that explain a high percentage of variance, 21.5%. Again, as in  $\text{PC1}_{18}$  (t) series, we observe an oscillatory pair with a dominant period of  $T \approx 6$  years. Furthermore we detect a quasioscillatory mode with a dominant period higher than decadal ( $T = 11.25$  years), accounting for 11% of the variance.

Fig. 5b shows the partial reconstruction,  $\text{REC}[12]$  (t) series, based on the pair T-PC1 and T-PC2 (T-EOF1 and T-EOF2) for the very low frequency oscillatory mode and the filtered  $\text{REC12[tot]}$  (t) series, which brings together reconstructions of the three oscillatory pairs found with SSA. It can be seen in  $\text{PC2}_{18}$  (t) time series an extended period of droughts between 1932 and 1957, while in the early twentieth century oscillatory cycles with  $T \approx 6$  years appear more differentiated. We can also determine a wet period from 1970 to 2000, where the low-frequency cycles (higher than decadal) dominate the series. The decline observed in  $\text{PC1}_{18}$  (t) at the beginning of 21st century is manifested as a consequence of a very low frequency cycle, with several years of moisture deficits since 2002, interrupted only between 2008 and 2009.

Fig. 4c shows the correlation pattern between the  $\text{PC3}_{18}$  (t), which accounts for the 8.6% of the total variance, with the  $\text{SPI}_{18}$  (t) series at each grid points. The correlation,  $a_{18,3}$ , changes from negative in the West and South of the region to positive in the Northeast extreme, with maximum values of 0.5. The  $\text{PC3}_{18}$  (t) time series is shown in Fig. 5c, where a highly fluctuating signal is observed, with cycles of irregular intensity more accentuated in the mid-twentieth century. This signal is partially reconstructed with the oscillatory pair captured by T-PC1 and T-PC2 from SSA, explaining 14.9% of the total variance with a dominant period  $T = 11.3$  years. The  $\text{PC3}_{18}$  (t) does not reflect any noticeable trend along the measurement period.

Fig. 4d summarizes the skill to reproduce the variability of  $\text{SPI}_{18}$  (t) series through the linear combination of the first PCs. It shows the cumulative variance that is accounted for by  $\text{PC1}_{18}$  (t),  $\text{PC2}_{18}$  (t) and  $\text{PC3}_{18}$  (t). In almost the totality of the region, except for small areas at the extremes NW and SW, the proportion of the total variance explained at each grid point is higher than 60%, that is, where the



**Fig. 6.** Proportion of NEA experiencing extremely wet conditions according to  $SEH_n(t)$  series,  $j=6, 12$  and  $18$  months. Solid lines denote the partial reconstructions corresponding to nonlinear trends,  $Ten[j](t)$ . (a)  $SEH_6(t)$  and  $Ten[6](t)$  accounting for 5.2% of the total variance, (b)  $SEH_{12}(t)$  and  $Ten[12](t)$  explaining 9.75% of the variance and (c)  $SEH_{18}(t)$  and  $Ten[18](t)$  (14% of the total variance).

behavior reproduced by the linear combination of the first components is considered satisfactory. It should be stressed that small isolated zones have total variances higher than 80%, whereas in most of the region, especially in the West-Central areas, the proportion of accounted variance is between 70 and 80%.

### 3.2. Spatial extent of extreme drought and wetness

We estimated the spatial extent of drought and wetness across NEA by constructing time series that calculate the percentage of grid points exceeding the thresholds of extremely wet or dry months (Table 1),  $SEH_n(t)$  and  $SED_n(t)$ ,  $n=6, 12$  and  $18$  months, respectively. The aim of this time series is to determine the fraction of the region experiencing water excess/deficit conditions at different time scales. Then, SSA was applied to the time series looking for significant signals in the LFB (trends or oscillatory modes). In order to evaluate the vulnerability of the region to EPE, we assessed the occurrence of situations with large portions of the entire study region under water excesses/deficit. A month when more than 50% of the total region exceeds a given threshold is defined as a wet/dry critical month (adapted from Krepper and Zucarelli, 2010). The areas of the NEA that were most affected by EPE and its average magnitude were delimited by mapping the average spatial distribution of  $SPI_n(t)$  series for critical months.

Fig. 6a–c shows  $SEH_n(t)$  time series ( $n=6, 12$  and  $18$  months) and the partial reconstruction for nonlinear trends,  $Ten[j](t)$  series, associated with each T-EOF1 and T-PC1 of the SSA, accounting for 5.2%, 9.75% and 14% of the total variance, respectively. Furthermore, we find an oscillatory cycle (not plotted) with  $T \approx 6.5$  years that explains 7.25%, 11.5% y 13.4% of the variance at each time scale (Table 3). It can be shown that all  $SEH_n(t)$  series present positive trends after mid-twentieth century. The largest amount of wet events with large spatial extent were found between 1972 and 2003, with extraordinary wetness in 1914–1915, 1973 and 2003. As in average areal behavior of  $SPI_n(t)$  series

**Table 3**

Trends and significant low-frequency oscillatory pairs obtained from applying SSA ( $M = 360$  months) to  $\text{SEH}_n(t)$  series,  $j = 6, 12$  and  $18$  month, with the percentage of explained variance and correlation coefficient  $R$ .

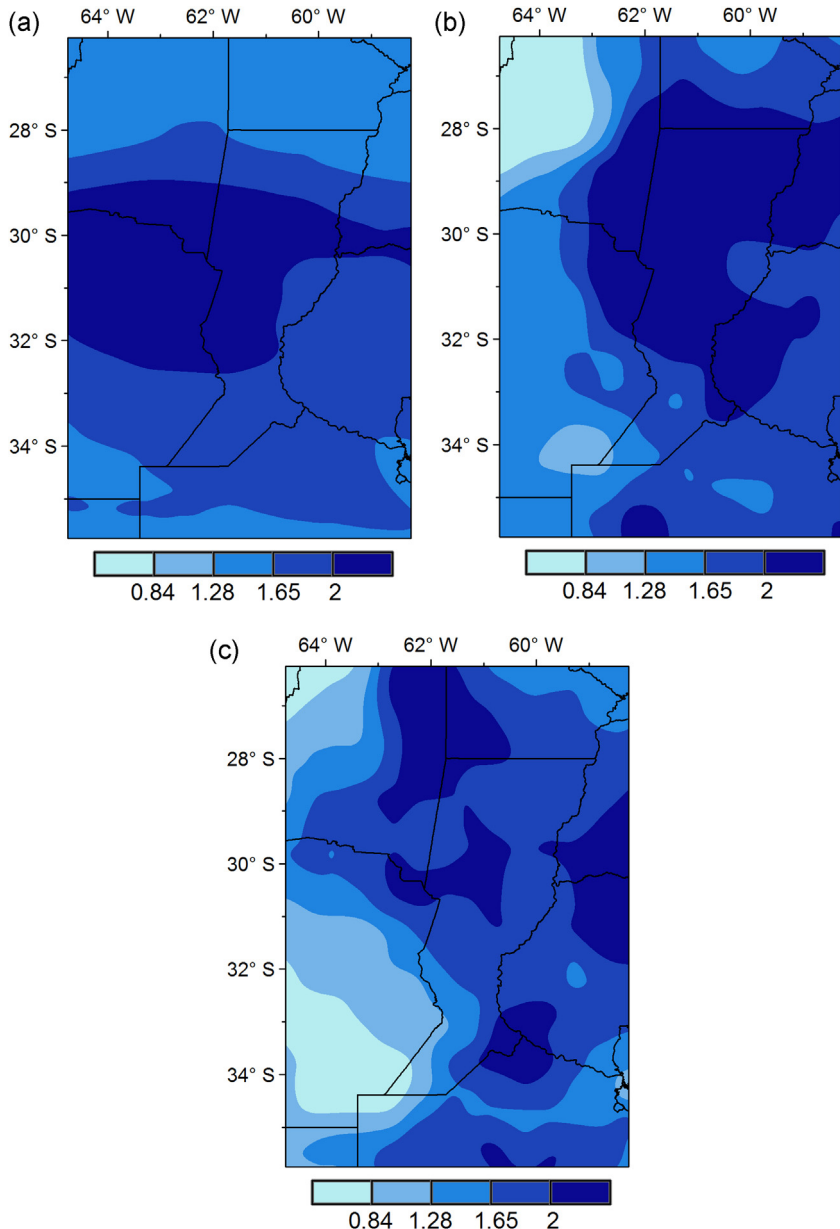
$\text{SEH}_n(t)$	Oscillatory pair (components)	Trend or dominant period (year/cycle)	Explained variance (%)	$R$ at lag $L$ (month)
$\text{SEH}_6(t)$	T-PC 1 T-PC2 and T-PC3 T-PCs [1 + 2 + 3]	Trend 6.6	5.1 7.25 12.35	$-0.987; L = 20$
$\text{SEH}_{12}(t)$	T-PC 1 T-PC2 and T-PC3 T-PCs [1 + 2 + 3]	Trend 6.6	9.75 11.45 21.2	$-0.970; L = 20$
$\text{SEH}_{18}(t)$	T-PC 1 T-PC2 and T-PC3 T-PCs [1 + 2 + 3]	Trend 6.6	14 13.4 27.4	$0.960; L = 19$

determined by  $\text{PC1}_n(t)$  patterns we can observe a trend reversal in  $\text{SEH}_n(t)$  series in the last years of the 2000s (noticeable at SPI scales of 12 and 18 months), suggesting that the wet EPE of larger spatial extent noted between 1970 and 2003 began to decline.

It should be emphasized that extremely wet periods that affect largest proportions of the NEA (Fig. 6a–c) are the same as those showing higher intensity and duration according to the temporal behavior of  $\text{PC1}_n(t)$  (Figs. 3a, b and 5a). In the SPI scales of 12 and 18 months hydrological extremely wet events of major temporal duration were observed in the period 1972–2003, with a maximum between June 1997 and January 2004 (80 consecutive months), both in spatial extent (Fig. 6b and c) and in magnitude (Figs. 3b and 5a). Furthermore, the peaks of 1973 and 2003 are consistent with a strong and a moderate El Niño events respectively, both according to the ONI series, while the peak of September 1915 corresponds to very low values of the SOI series.

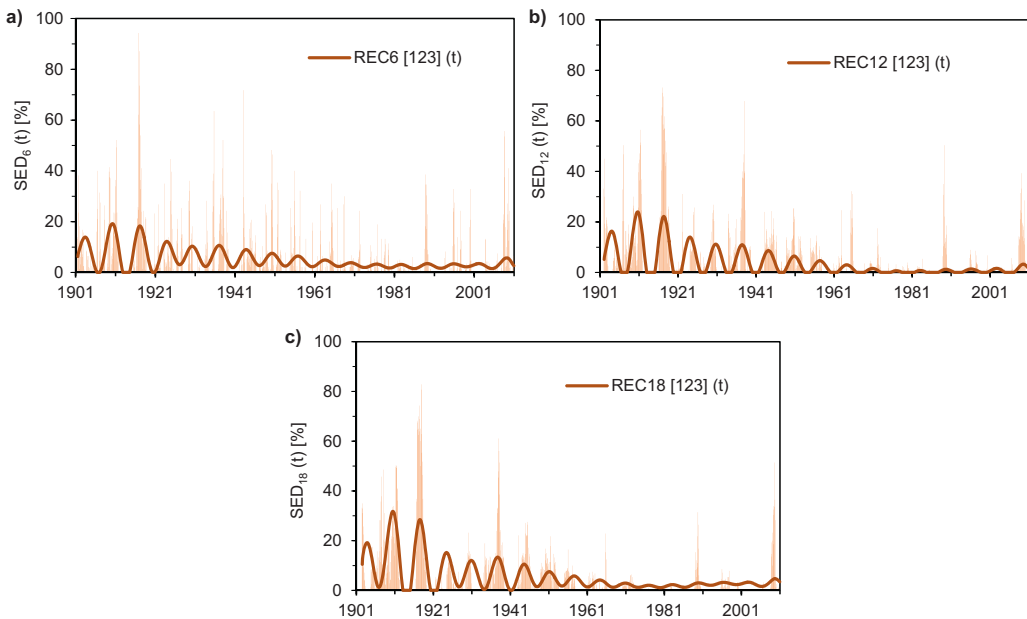
Fig. 7a–c shows the average spatial behavior of  $\text{SPI}_n(t)$  series in extremely wet critical months. At scale of six months, most of the region experienced extremely wet conditions, except for the North and a small portion of the South with very wet conditions (Fig. 7a). We must make clear that, in this paper we assume the threshold  $\text{SPI}_n(t) > 2$  ( $\text{SPI}_n(t) < -2$ ) to define an extraordinary wet (dry) EPE instead the scale of intensities given by McKee et al. (1993) that uses these threshold to define extremely dry (wet) events. Fig. 7a shows a delimited area with  $\text{SPI}_6(t) > 2$  that covers the North-Central Santa Fe, South of Corrientes, Northern Córdoba and South of Santiago del Estero provinces in Argentina vulnerable to extraordinary wet events at a relevant scale to agricultural decisions. Fig. 7a presents a West-East gradient, with Midwestern region experiencing extremely wet conditions and mainly the Centre-North of Santa Fe province being the most affected area by extraordinary wet EPE at the 12 month time scale. It should be noted that in the Western area the conditions during critical months were moderately wet and normal in the Northwest corner of the study region. Hydrological conditions for critical months, represented by the low-frequency behavior of the  $\text{SPI}_{18}(t)$  series average in critical months (Fig. 7c), are almost the same as Fig. 7b, except for isolated areas experiencing extraordinary wet extreme conditions and an expansion of the region with normal behavior in the Southwest extreme of NEA.

Fig. 8a–c illustrates time series for the proportion of NEA experiencing extreme drought conditions as defined by  $\text{SED}_n(t)$ ,  $n = 6, 12$  and  $18$  months. The low frequency signals detected by SSA are set out in Table 4. For all time scales analyzed, we identify an oscillatory cycle with a dominant period  $T \approx 6.6$  years and a negative nonlinear trend (not plotted). Partial reconstructions associated with the first three T-EOFs and T-PCs from SSA for each time scale are shown in Fig. 8a–c. It can be seen that the magnitude of the oscillatory pair increments for time scales increasing from 6 to 18 months. Furthermore, the oscillatory mode is particularly significant in the early 20th century, gradually decreasing in frequency, with the lowest magnitude in the wet period (1970–2000) and recovering slightly relevance in the 2000s.



**Fig. 7.** Average spatial behavior of  $\text{SPI}_n(t)$  series for critical months (more than 50% of the region exceeds the threshold) for extremely wet conditions ( $\text{SPI}_n(t) > 1.65$ ) at time scales of: (a)  $n = 6$  months, (b)  $n = 12$  months and (c)  $n = 18$  months.

The  $\text{SED}_6(t)$  series (Fig. 8a) emphasizes seasonal variations, representing droughts of greater importance for the agricultural sector. The maximum value of the series was in November 1916, where 94% of the region experienced extreme drought conditions. It can be observed that most of the agricultural droughts, both in spatial extent and in magnitude (Fig. 3a) were between 1901 and 1960. The behavior of hydrological droughts, represented by the  $\text{SED}_{18}(t)$  series, is presented in Fig. 8c. In the worst drought of the twentieth century there were 17 consecutive critical months, between October



**Fig. 8.** Proportion of NEA experiencing extremely dry conditions according to  $SED_n(t)$  series,  $j=6, 12$  and  $18$  months. Solid lines denote the partial reconstructions corresponding to the oscillatory cycle with a dominant period  $T \approx 6.6$  years and the negative nonlinear trend (Table 4). (a)  $SED_6(t)$  and  $REC6[123](t)$  (accounting for 14% of the total variance), (b)  $SED_{12}(t)$  and  $REC12[123](t)$  (29.5% of the variance) and (c)  $SED_{18}(t)$  and  $REC12[123](t)$  (36.7% of the total variance).

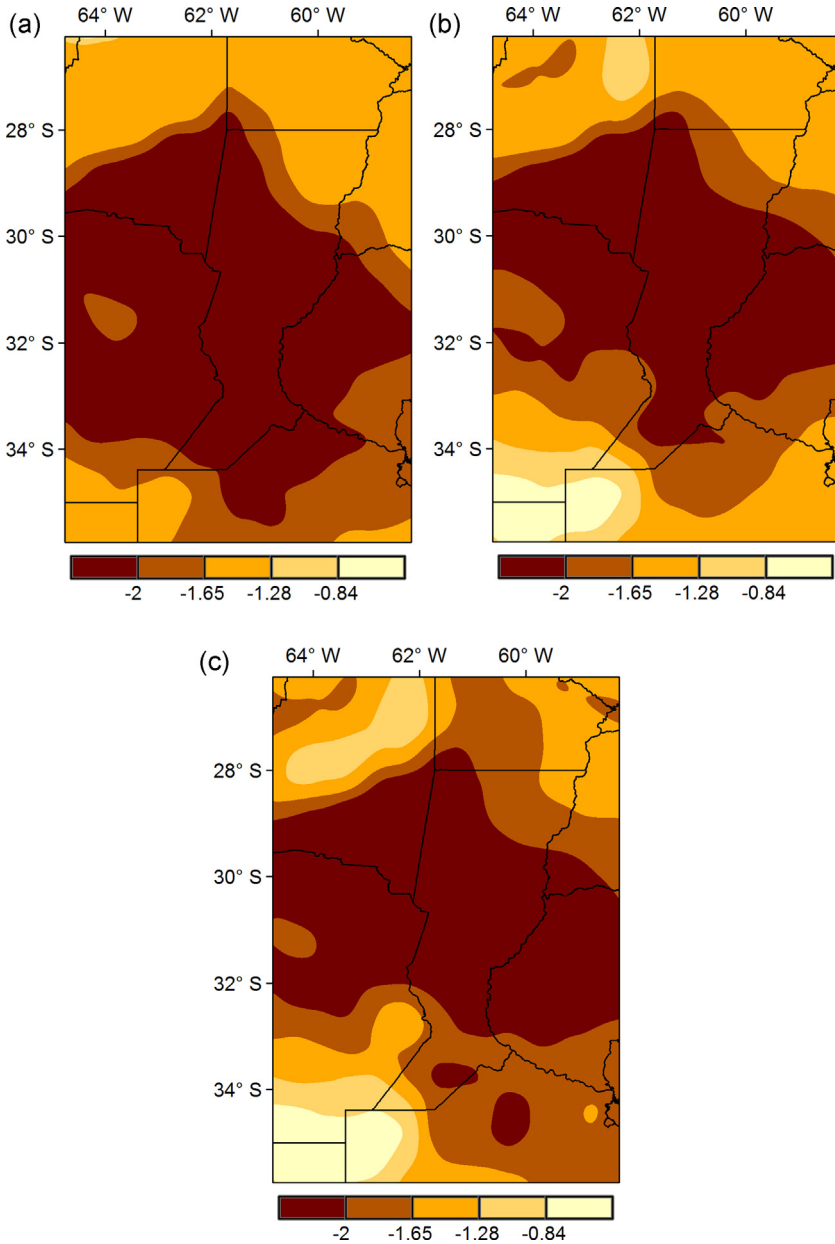
1916 and February 1918, with 83% of the entire region under hydrological extreme dry conditions ( $SPI_{18}(t) < -1.65$ ) in December 1917, consistent with the most intense La Niña event of 20th century according to SOI time series. Other important events, both in spatial extent and intensity (Fig. 5a), were recorded in 1937–1938, 1907–1911 and 2007–2008.

Fig. 9a–c shows the average spatial behavior of  $SPI_n(t)$  series in extremely dry critical months. The area affected by extraordinary extreme dry conditions ( $SPI_n(t) < -2$ ) depends on time scales, being more extensive in the intra-annual scale (6 months) and decreasing to the central zone of the region at longer time scales (12 and 18 months). Conversely, the extremely dry region, which occupies

**Table 4**

Trends and significant low-frequency oscillatory pairs obtained from applying SSA ( $M = 360$  months) to  $SED_n(t)$  series,  $j=6, 12$  and  $18$  month, with the percentage of explained variance and correlation coefficient  $R$ .

$SED_n(t)$	Oscillatory pair (components)	Trend or dominant period (year/cycle)	Explained variance (%)	$R$ at lag $L$ (month)
$SED_6(t)$	T-PC1 and T-PC2	6.6	9.7	-0.881; $L=21$
	T-PC3	Trend	4.3	
	T-PCs [1 + 2 + 3]		14	
$SED_{12}(t)$	T-PC1 and T-PC2	6.6	20.6	-0.843; $L=20$
	T-PC3	Trend	8.9	
	T-PCs [1 + 2 + 3]		29.5	
$SED_{18}(t)$	T-PC1	Trend	13.1	0.958; $L=21$
	T-PC2 and T-PC3	6.6	23.6	
	T-PCs [1 + 2 + 3]		36.7	



**Fig. 9.** Average spatial behavior of  $\text{SPI}_n(t)$  series ( $t$ ) for critical months (more than 50% of the region exceeds the threshold) with extremely dry conditions ( $\text{SPI}_n(t) < -1.65$ ) at time scales of: (a)  $n = 6$  months, (b)  $n = 12$  months and (c)  $n = 18$  months.

most of the South-Central area at time scales of 6 and 12 months, increases toward the north and decreases in the SW extreme at the low frequency scale of 18 months. The most vulnerable area to extraordinary extreme hydrological droughts, represented by the portion with  $\text{SPI}_{18}(t) < -2$  (Fig. 9c), includes the North-Central zones of Entre Ríos, Santa Fe and Córdoba, South of Santiago del Estero and SW of Corrientes provinces. The Southwestern corner shows average normal conditions during critical months of the study period, similar to the scale of 12 months (Fig. 9b). Most of the region,

except for the northern portion above 28° S, shows a significant vulnerability to extreme dry events at intra-annual time scale, relevant for agriculture (Fig. 9a), with a large area experiencing extraordinary extreme droughts in critical months between 1901 and 2010.

#### 4. Discussion

Our results showed that low-frequency behavior of EPE in the NEA was differentiated into two distinct periods: a dry one between 1901 and 1960 and a wet one between 1970 and 2003. This behavior is associated with well-known long-term changes in precipitation starting in the 1950s and reported by several authors (e.g., [Minetti and Vargas, 1998](#); [Krepper and Sequeira, 1998](#); [Krepper and Garcia, 2004](#)). The time series of SPI and wetness area coverage analyzed at different time scales, presents signs of stabilization and a trend reversal toward drier conditions since 2007. These results are consistent with those reported by [Seager et al. \(2010\)](#) for the whole SESA region. They argue that while the long-term trend toward wetter conditions in SESA was of great benefit to regional agriculture, there is no reason to expect this to continue since it seems to have been influenced by tropical SST anomalies associated with the AMO. This index is presumed to be shifting toward a positive phase ([Ting et al., 2009](#)) that may force a decrease in SESA precipitation in the coming years. These implications and the results presented in this paper presumably indicate that hydrological wet EPE of high intensity, duration and spatial extent noticed between 1970 and 2003 could decline in the coming years.

[Viglizzo and Frank \(2006\)](#) described a large drought episode in the 1930s and 1940s denoted as the “Pampas Dust Bowl” in the Western Pampas of Argentina. In our paper, the behavior of SPI fields and the area covered by droughts showed a dry period in the center of the study region between about 1925 and 1940 and for the Northwest extreme between 1930 and 1950 that might extend the “Pampas Dust Bowl” to the bulk of the NEA. The 1930s drought appears within a hemispherical symmetric pattern of precipitation anomalies across the Americas with drought in both the northern and southern extratropics. Unlike the North American Dust Bowl, the Pampas Dust Bowl does not appear strongly tied to the La Niña conditions but to the tropical Atlantic Ocean which was then warm and which is expected to favor dry conditions in SESA ([Seager et al., 2010](#)).

The drought and wetness hydrological behavior reproduced by the linear combination of the first components of PCA applied to SPI field at scale of 18 months is considered satisfactory since, in almost the totality of the NEA, the proportion of the total variance explained at each grid point was higher than 60%. The implementation of SSA allowed us to find a common oscillatory cycle for SPI and drought/wetness spatial coverage series with a dominant period of about 6.5 years, both for dry and wet events, so we could infer that EPE, in spatial extent and in intensity have the same leading periodicities. Consistently with these results, [Krepper and Garcia \(2004\)](#) reported a cycle of  $T \approx 6$  years in monthly precipitation series for the whole LPB and for gauging stations on the Uruguay River. Another important hydrological cycle in SPI series at 18 month time scale was the oscillatory mode with dominant period of  $T = 8.7$  years. This result is consistent with a quasi-decadal cycle found in the annual streamflow of the Paraná and Paraguay rivers reported by [García and Mechoso \(2005\)](#) and [Robertson and Mechoso \(1998\)](#), who associated this cycle with SST anomalies situated over the tropical North Atlantic. In addition, [Venencio and García \(2012\)](#) detected a similar cycle (close to 8 years) in annual precipitation in the South of the province of Santa Fe.

As could be expected, extremely dry and wet periods that affect the largest areas of the NEA, considering the percentage of grid points that exceed the thresholds of extremely wet or dry months, were the same as those showing EPE of higher intensity and duration according to the temporal behavior given by SPI field at different time scales. The analysis of historical events with large portions of the entire region under water excess/deficit at critical months enabled us to determine the most vulnerable zones to extreme drought/wetness. The implications of these results depend on which time scales are used. The shorter scales ( $n = 6$  months) provide valuable information for decision-making in livestock and crop production, while the longer period time scales ( $n = 12$  or 18 months) describe the hydrological behavior of the region. The exploration at all time scales indicates that the Central-West portion of NEA seems to be the most vulnerable area to extraordinary extreme drought/wetness.

## 5. Conclusions

We have presented the spatiotemporal behavior of EPE observed throughout the 20th century and up to the year 2010 in the NEA. Dry and wet events were characterized by means of the SPI applied to monthly precipitation series at different time scales (6, 12 and 18 months). Given that the stations in NEA are not homogeneously distributed in space we used gridded precipitation datasets on high-resolution. The dataset CRU TS 3.2 and GPCC v6 were validated with observed precipitation data and the latter was selected because it best fit extreme observed fluctuations and satisfy the reliability criteria of climate data to investigate dry/wet periods (Bordi et al., 2006).

The first PC from PCA applied to SPI fields explained a high percentage of the total variance at all time scales analyzed and represented its average areal behavior. In  $PC_{1n}(t)$  time series,  $n = 6, 12$  and  $18$  months, the T- $PC_1$  from SSA was associated with a positive nonlinear trend, whose low frequency behavior showed changes to wetter conditions from 1960 to 2000s, subsequent signs of stabilization and a trend reversal since the first decade of 21st century. The largest and more severe hydrological and agricultural droughts in the NEA occurred between 1901 and 1960 while a period of wet EPE of long duration and high intensity was recorded between years 1970 and 2005, causing the worst floods of the 20th century. Moreover, an extended period with very dry conditions was registered between 1921 and 1939 that might extend the “Pampas Dust Bowl” to the bulk of the NEA.

Almost the entire NEA—except the Northwestern corner—showed  $SPI_{18}(t)$  series whose low-frequency time response presented a nonlinear positive trend and oscillatory pairs with dominant periods  $T = 6.5$  years and  $8.7$  years, determining the periodicity of EPE in the region. The Northwestern corner of the study region showed a possible oscillatory pair of very low frequency, an important cycle of 6 years and a quasioscillatory mode with  $T = 11.25$  years/cycle. Our results showed that the linear combination of  $PC_{18}(t)$ ,  $PC_{218}(t)$  and  $PC_{318}(t)$  allowed an adequate reproduction of a high percentage of low frequency variance of EPE over an extensive area of NEA, especially in the West-Central zone, where the proportion of accounted variance was between 70 and 80%.

The low frequency behavior of wetness area coverage time series showed a remarkable nonlinear trend, particularly at longer time scales, with a trend reversal in the last years of the 2000s. This feature is similar to that found in the average areal behavior of SPI fields, suggesting that wet EPE of higher severity noted between 1970 and 2003 begin to decline. The most intense hydrological extremely wet events were recorded in the wet period of the late 20th century, with extraordinary peaks in October 1973 (consistent with strong El Niño event) and March 2003 (consistent with a moderate El Niño event). This last event caused the most catastrophic flood of the Salado Basin. On the other hand, no well-defined nonlinear negative trends were found in drought area coverage time series. Instead, this last series, presented an important oscillatory cycle with a dominant period of 6 years, showing a periodicity of extremely drought condition in the region, particularly differentiated in the first half of the 20th century. The worst hydrological drought of the 20th century was observed between October 1916 and February 1918 with 17 consecutive critical months and 83% of the whole region remained under hydrological extreme dry conditions in December 1917. This event is consistent with a strong La Niña event. The last great extreme hydrological drought in NEA, which caused serious damage to the economic activities of the region, occurred between 2008 and 2009.

During extremely wet critical months a general West-East gradient of SPI fields was observed, with extremely wet conditions in Midwestern NEA, moderately wet in the Western area and normal in the Northwest corner. In extremely dry critical months, the area affected by extreme dry conditions depended on time scales, occupying most of the South-Central area at time scales of 6 and 12 months and increasing toward the north and decreasing in the SW corner at the scale of 18 months. The most vulnerable area for both extremely wet and dry events at hydrological scale was the Central West portion of NEA. Most of the entire NEA, except for the northern portion above  $28^{\circ}$  S, showed significant vulnerability to extreme both, dry and wet events at time scale of 6 months, which is most relevant for agricultural activities.

The NEA is one of the most productive regions, particularly in annual crops and livestock, so that good information on drought (wetness) risk should help to improve climate risk management. This paper provides information for improved understanding of the spatiotemporal features of EPE relevant to assist in decision-making and to improve adaptation and risk management policies and practices.

Our results suggest that the NEA (especially the Central-West portion) is highly vulnerable to extreme dry/wet precipitation events, and therefore it is necessary to implement proper water resource management strategies for achieving sustainability, emphasizing in actions to prevent and minimize the negative impacts of droughts and floods.

## Acknowledgements

We thank Andrew Robertson, Arthur M. Greene and Angel Muñoz for their advice in the early stages of the paper. We thank Hugo Berbery and an anonymous reviewer for their comments and corrections that helped to improve the paper. Miguel Lovino is supported by a Postgraduate Studentship from the Argentinian National Scientific and Technical Research Council (CONICET). This research was partially supported by a grant from the Secretary of Science and Technology of the Universidad Nacional del Litoral (Project C.A.I. + D. 2011 N° 35/180).

## References

- Anderson, O.D., 1977. *Time Series Analysis and Forecasting*. Butterworths, UK.
- Agnew, C., 2000. *Using the SPI to identify drought*. Drought Netw. News 12, 6–12.
- Berbery, E., Barros, V., 2002. *The hydrologic cycle of the La Plata basin in South America*. *J. Hydrometeorol.* 3, 630–645.
- Bordi, I., Fraedrich, K., Jiang, J.-M., Sutera, A., 2004. Spatio-temporal variability of dry and wet periods in eastern China. *Theor. Appl. Climatol.* 79, 81–91.
- Bordi, I., Fraedrich, K., Petitta, M., Sutera, A., 2006. Large-scale assessment of drought variability based on NCEP/NCAR and ERA-40 re-analyzes. *Water Resour. Manage.* 20, 899–915.
- Bordi, I., Fraedrich, F., Sutera, A., 2009. Observed drought and wetness trends in Europe: an update. *Hydrol. Earth Syst. Sci.* 13, 1519–1530.
- Bordi, I., Sutera, A., 2012. Drought assessment in a changing climate. In: Hannachi, A. (Ed.), *Climate Variability – Some Aspects, Challenges and Prospects*. InTech, ISBN: 978-953-307-699-7. Available from: <http://www.intechopen.com/books/climate-variability-some-aspects-challenges-and-prospects/drought-assessment-in-a-changing-climate>
- Caffera, R.M., Berbery, E.H., 2006. *La Plata basin climatology*. In: Barros, V., Clarke, R., Diaz, P. (Eds.), *Climatic change in the La Plata basin*. National Scientific and Technical Research Council (CONICET), Argentina, pp. 16–32.
- Cavalcanti, I., Carril, A., et al., 2011. CLARIS LPB WP6: processes and future evolution of extreme climate events in La Plata Basin. *CLIVAR Exch.* 57, 22–24.
- Chatfield, C., 2004. *The Analysis of Time Series, an Introduction*, sixth ed. Chapman & Hall/CRC, New York.
- ECLAC (United Nations Economic Commission for Latin America and the Caribbean), 2003. *The Floods of 2003 in Santa Fe, Argentina*, [http://www.gfdrr.org/sites/gfdrr.org/files/dldocs/\(2003\)Las%20inundaciones,%20Santa%20Fe%20Argentina%20\(ESP\).pdf](http://www.gfdrr.org/sites/gfdrr.org/files/dldocs/(2003)Las%20inundaciones,%20Santa%20Fe%20Argentina%20(ESP).pdf) (accessed December 2013).
- Coronel, G., Menéndez, G., 2006. *Physiography and hydrology*. In: Barros, V., Clarke, R., Diaz, P. (Eds.), *Climatic Change in the La Plata Basin*. National Scientific and Technical Research Council (CONICET), Argentina, pp. 44–59.
- Edwards, D., McKee, T., Climatology Report No. 97-2 1997. *Characteristics of 20th Century Drought in the United States at Multiple Timescales*. Colorado State University, Fort Collins, 155 pp.
- Fischer, T., Gemmer, M., Su, B., Scholten, T., 2013. Hydrological long-term dry and wet periods in the Xijiang River basin, South China. *Hydrol. Earth Syst. Sci.* 17, 135–148.
- García, N.O., Vargas, W.M., 1998. The temporal climatic variability in the Río de la Plata basin displayed by the river discharges. *Clim. Change* 38, 359–379.
- García, N., Mechoso, C., 2005. *Variability in the discharge of South American rivers and in climate*. *Hydrol. Sci. J.* 50, 459–477.
- Ghil, M., Allen, M., Dettinger, M., Ide, K., Kondrashov, D., Mann, M., Robertson, A., Saunders, A., Tian, Y., Varadi, F., Yiou, P., 2001. *Advanced spectral method for climatic time series*. *Rev. Geophys.* 40, 1–41.
- Guttmann, N., 1999. Accepting the standardised precipitation index: a calculation algorithm. *J. Am. Water Resour. Assoc.* 35, 311–322.
- Hayes, M., Svoboda, M., Wilhite, D., Vanyarkho, O., 1999. Monitoring the 1996 drought using the standardized precipitation index. *Bull. Am. Meteorol. Soc.* 80, 429–438.
- Hayes, M., Svoboda, M., Wall, N., Widhalm, M., 2011. The Lincoln declaration on drought indices: universal meteorological drought index recommended. *Bull. Am. Meteorol. Soc.* 92, 485–488.
- Jones, P., Harris, I., 2012. CRU Time Series High Resolution Gridded Data Version 3.2. NCAS British Atmospheric Data Centre, University of East Anglia Climatic Research Unit (CRU), Available at: [http://badc.nerc.ac.uk/view/badc.nerc.ac.uk\\_ATOM\\_ACTIVITY\\_3ec0d1c6-4616-11e2-89a3-00163e251233](http://badc.nerc.ac.uk/view/badc.nerc.ac.uk_ATOM_ACTIVITY_3ec0d1c6-4616-11e2-89a3-00163e251233)
- Keyantash, J., Dracup, J.A., 2002. The quantification of drought: an evaluation of drought indices. *Bull. Am. Meteorol. Soc.* 83, 1167–1180.
- Krepper, C., García, N., 2004. Spatial and temporal structures of trends and interannual variability of precipitation over the La Plata Basin. *Q. Int.* 114, 11–21.
- Krepper, C., Sequeira, M., 1998. Low-frequency variability of rainfall in Southeastern South America. *Theor. Appl. Climatol.* 61, 19–28.
- Krepper, C.M., Zucarelli, G.V., 2010. Climatology of water excesses and shortages in the La Plata Basin. *Theor. Appl. Climatol.* 102, 13–27.

- Livada, I., Assimakopoulos, V.D., 2007. Spatial and temporal analysis of drought in Greece using the Standardized Precipitation Index (SPI). *Theor. Appl. Climatol.* 89, 143–153.
- Lloyd-Hughes, B., Saunders, M., 2002. A drought climatology for Europe. *Int. J. Climatol.* 22, 1571–1592.
- Magrin, G., Gay García, C., Cruz Choque, D., Giménez, J.C., Moreno, A.R., Nagy, G.J., Nobre, C., Villamizar, A., 2007. In: Parry, M.L., Canziani, O.F., Palutikoff, J.P., van der Linden, P.J., Hanson, C.E. (Eds.), Latin America. *Climate Change 2007: Impacts, Adaptation and Vulnerability. Contribution of Working Group II to the Fourth Assessment Report of the Intergovernmental Panel on Climate Change*. Cambridge University Press, Cambridge, UK, pp. 581–615.
- McKee, T., Doesken, N., Kleist, J., 1993. The relation of drought frequency and duration to time scales. In: Proceeding of the Eight Conference on Applied Climatology, Anaheim, CA, 17–22 January. Amer. Meteor. Soc., Boston, MA, pp. 179–184.
- Meehl, G., Covey, C., Delworth, T., Latif, M., McAvaney, B., Mitchell, J.F.B., Stouffer, R.J., Taylor, K.E., 2007. The WCRP CMIP3 multimodel dataset: a new era in climate change research. *Bull. Am. Meteorol. Soc.* 88, 1383–1394.
- Minetti, J., Vargas, W., 1998. Trends and jump in the annual precipitation in South America, south of the 15°S. *Atmósfera* 11, 205–221.
- NOAA/NWS/CPC, Oceanic Niño Index (ONI). NOAA National Weather Service, Center for Climate Prediction. Available at: [http://www.cpc.ncep.noaa.gov/products/analysis\\_monitoring/ensostuff/ensoyears.shtml](http://www.cpc.ncep.noaa.gov/products/analysis_monitoring/ensostuff/ensoyears.shtml) (accessed March 2014).
- Paegle, J., Mo, K., 2002. Linkages between summer rainfall variability over South America and sea surface temperature anomalies. *J. Clim.* 15, 1389–1407.
- Raziei, T., Bordi, I., Pereira, L., Sutera, A., 2010. Space-time variability of hydrological drought and wetness in Iran using NCEP/NCAR and GPCC datasets. *Hydrol. Earth Syst. Sci.* 14, 1919–1930.
- Remenieras, G., 1974. *Tratado de Hidrología Aplicada*. Editores Técnicos asociados S.A., Barcelona, España.
- Robertson, A., Mechoso, C., 1998. Interannual and decadal cycles in river flows of southeastern South America. *J. Clim.* 11, 2570–2581.
- Santos, J., Pulido-Calvo, I., Portela, M., 2010. Spatial and temporal variability of droughts in Portugal. *Water Resour. Res.* 46, W03503, <http://dx.doi.org/10.1029/2009WR008071>.
- Schneider, U., Becker, A., Finger, P., Meyer-Christoffer, A., Rudolf, B., Ziese, M., 2011. GPCC Full Data Reanalysis Version 6.0 at 0.5°: Monthly Land-Surface Precipitation from Rain-Gauges built on GTS-based and Historic Data. [http://dx.doi.org/10.5676/DWD\\_GPCC/FD\\_M.V6.050](http://dx.doi.org/10.5676/DWD_GPCC/FD_M.V6.050).
- Seager, R., Naik, N., Baethgen, W., Robertson, A., Kushnir, Y., Nakamura, J., Jurburg, S., 2010. Tropical oceanic causes of interannual to multidecadal precipitation variability in southeast South America over the past century. *J. Clim.* 23, 5517–5539.
- Sönmez, F., Kömüscü, A., Erkan, A., Turgu, E., 2005. An analysis of spatial and temporal dimension of drought vulnerability in turkey using the standardized precipitation index. *Nat. Hazards* 35, 243–264.
- Sirdaş, S., Şen, K., 2003. Spatio-temporal drought analysis in the Trakya region, Turkey. *Hydrol. Sci. J.* 48, 809–820.
- Telesca, L., Vicente-Serrano, S., López-Moreno, J., 2013. Power spectral characteristics of drought indices in the Ebro river basin at different temporal scales. *Stochast. Environ. Res. Risk Assess.* 27, 1155–1170.
- Ting, M., Kushnir, Y., Seager, R., Li, C., 2009. Forced and internal twentieth-century trends in the North Atlantic. *J. Clim.* 22, 1469–1481.
- Trenberth, K.E., Hoar, T.J., 1996. The 1990–1995 El Niño–Southern oscillation event longest on record. *Geophys. Res. Lett.* 23, 57–60.
- Vera, C., Barange, M., Dubec, O.P., Goddard, L., Griggse, D., Kobysheva, N., Odadag, E., Pareyh, S., Polovinai, J., Povedaj, G., Seguin, B., Trenberth, K., 2010. Needs assessment for climate information on decadal timescales and longer. *Proc. Environ. Sci.* 1, 275–286.
- Venencio, M.V., García, N., 2005. Impacto de las sequías en la recarga natural al acuífero libre. *Rev. Bras. Recur. Hídric.* 10, 49–60.
- Venencio, M.V., García, N., 2012. Interannual variability and predictability of water table levels at Santa Fe Province (Argentina) within the climatic change context. *J. Hydrol.* 409, 62–70.
- Vicente-Serrano, S., 2006. Spatial and temporal analysis of droughts in the Iberian Peninsula (1910–2000). *Hydrol. Sci. J.* 51, 83–97.
- Viglizzo, E., Frank, F.C., 2006. Ecological interactions, feedbacks, thresholds and collapses in the Argentine Pampas in response to climate and farming during the last century. *Q. Int.* 158, 122–126.
- Von Storch, H., Navarra, A., 1995. *Analysis of Climate Variability*. Springer-Verlag Berlin Heidelberg, Germany.
- Von Storch, H., Zwiers, W., 1999. *Statistical Analysis in Climate Research*. Cambridge University Press, USA.
- Wilks, D.S., 2006. *Statistical Methods in the Atmospheric Sciences*. Elsevier Inc., UK.
- Wilhite, D.A., 2000. Drought as a natural hazard: concepts and definitions. In: Wilhite, D.A. (Ed.), *Drought: A Global Assessment*. Routledge, New York, USA, pp. 1–18.
- WMO, 2008. *Guide to Hydrological Practices*, WMO No. 168. World Meteorological Organization, Genève, Switzerland.
- Zhai, J., Su, B., Krysanova, V., Vetter, T., Gao, C., Jiang, T., 2010. Spatial variation and trends in PDSI and SPI indices and their relation to streamflow in 10 large regions of China. *J. Clim.* 23, 649–663.